A special synthesis of BiOCl photocatalyst for efficient pollutants removal: New insight into the band structure regulation and molecular oxygen activation

Han Zhao, Xiang Liu*, Yuming Dong, Yongmei Xia, Haijun Wang

Key Laboratory of Synthetic and Biological Colloids, Ministry of Education, School of Chemical and Material Engineering, Jiangnan University, Wuxi 214122, PR China

ABSTRACT

Exploitation of efficient photocatalytic materials is a vital matter to settle the energy and environmental crisis we are facing. In this work, BiOCl with oxygen vacancy (OV-BOC) is synthesized by solvothermal modification method. According to the acquired DRS, VB-XPS, ESR results, solvothermal modification synthesis can not only introduce oxygen vacancy which supports the generation of $^1O_2$ but regulate the band structure, giving rise to the valance band down-shift and hence the photogenerated h^+ possesses higher oxidation capacity, which brings about desirable photodegradation efficiency on organic pollutants. It is unexpected that the degradation rate can be promoted by 2.6, 3.1 and 2.4 times after adding a little H_2O_2 towards rhodamine B, methyl orange and phenol, respectively, which benefits from the increased production of $·O_2^-$. These increased $·O_2^-$ comes from activated H_2O_2 through the direct attack of holes which possesses higher oxidation capacity because of valance band down-shift $(H_2O_2 + h^+ \rightarrow ·O_2^- + 2H^+)$, as certified by analyses of free radicals and band positions. Radical species capturing and ESR experiments are used to reveal the mechanisms involved by reactive oxygen species and the results show that h^+, $^1O_2$ and $·O_2^-$ species are all responsible for photocatalytic degradation. This study may give some guidance on architecting photocatalysts on band structure regulation and molecular oxygen activation simultaneously.

1. Introduction

Along with the rapid expansion of industrialization, the exploration for efficient photocatalysts to address environmental issues has long been considered as a huge challenge over the past decades [1–4]. So far a great many photocatalytic materials have been developed and exhibited great potential in energy conversion [5,6] and environmental remediation [7–9], such as TiO_2 [10–15], g-C_3N_4 [16–18], MOFs-based materials [19–23] and so on. Very recently, tetragonal BiOCl appeals to extensive interest of researchers by virtue of unique layered structure which can induce the appearance of built-in electric field along [001] direction, thereby effectively promoting charge separation and transfer [24,25]. Nevertheless, the deficient photoabsorption towards visible light limits its practical application. Accordingly, several strategies such as fabricating heterojunctions [26,27], depositing noble metals [28], doping heteroatoms [29,30] and so on have been adopted to over this shortcoming. Previous research shows that introducing defects into materials can serve as electron trap center which further improve the separation efficiency of photogenerated carriers [31]. Especially for

oxygen vacancy, a typical defect, the introduction can create a defect level which decreases the band gap and activates O_2 to produce $·O_2^-$, O_2^{2-} and O_4^{2-} for further photocatalytic process [32–34].

Generally, these reactive oxygen species (ROS) involve in surface reactions are of critical significance in chemistry, biology, food and so on [35,36]. To be specific, ROS often serve as reaction intermediates that affect reaction process to a great extent. Accordingly, exploration of ROS favors the better acquaintance of the reaction mechanism. However, the deficient awareness between oxygen vacancy and ROS ($^1O_2$, $·O_2^-$ and $·OH$) is still ill-defined. For this, overall apprehension and consideration of ROS are indispensable when architecting photocatalysts to achieve efficient photocatalytic activity.

Furthermore, H_2O_2, known as a strong oxidant, is widely applied in photocatalysis and Fenton degradation [37,38]. For Fenton systems, $·OH$ can be activated by Fe^{3+} to achieve efficient degradation ability towards organic pollutants. But the concrete process and mechanism of H_2O_2 participating in photocatalysis about whether $·OH$ solely or other ROS involved in the reaction remain unclear and debatable [39]. Therefore, in-depth investigation of reactions involved by H_2O_2 and the

correlation of H_2O_2 may be a significant and meaningful work.

In addition to above-mentioned oxygen vacancy, ROS and H_2O_2, the potentials of conduction band and valance band of photocatalysts also contribute to photocatalytic ability. However, conventional methods such as heterojunction and elemental doping engineering can not realize adjustable band positions [40]. So it is necessary to develop a gentle approach to regulate the energy band position especially for these materials with oxygen vacancy to satisfy high photocatalytic efficiency.

Consequently, we expected to adjust the conduction band or valance band in the preparation process of BiOCl with oxygen vacancy and simultaneously generate more ROS through the involvement of H_2O_2 when necessary to enhance photocatalytic performance, in which complicated methods such as fabrication of 2D-2D BiOCl-OV/g-C_3N_4 could be avoided [41]. Hence, BiOCl with oxygen vacancy (OV-BOC) is synthesized by a special solvothermal modification method which can greatly affect the structure, band position of the BiOCl, as validated by ESR, VB-XPS and other characteristic methods in our study. In addition, oxygen vacancy defect in OV-BOC sample caused by special solvothermal method may present a close relation with the production of $^1O_2$, a common ROS, which is also favorable for photocatalytic degradation. Moreover, the results also show that the as-obtained OV-BOC sample exhibits an activation effect of H_2O_2 by photogenerated holes with higher oxidation capacity by virtue of valance band position down-shift to generate more $\cdot O_2^-$ which leads to the 2–3 times promotion in photodegradation efficiency towards different pollutants. This work may provide new vision in regulating energy band structure and activating molecular oxygen for the design of photocatalysts.

2. Experimental section

2.1. Chemicals

Barium nitrate pentahydrate ($(Bi(NO_3)_3 \cdot 5H_2O)$, sodium chloride (NaCl), hydrogen peroxide (H_2O_2), potassium hydroxide (KOH), ethanol (EtOH), ethylene glycol (EG), terephthalic acid (TA), nitro blue tetrazolium (NBT), 5,5-dimethyl-1-pyrroline N-oxide (DMPO), 3,3′,5,5′-tetramethylbenzidine (TEMP), rhodamine B (RhB), methyl orange (MO) and phenol were obtained from Sigma-Aldrich. Deionized water was utilized throughout the whole experiment.

2.2. Experimental

2.2.1. Preparation of BiOCl with oxygen vacancy

1 mmol $Bi(NO_3)_3 \cdot 5H_2O$ and NaCl were added to 30 mL EG accompanied by strong magnetic stirring, respectively. After dissolving, the above suspensions were mixed up and then transferred to Teflon-lined stainless autoclave and heated at 160 °C with the duration of 16 h. After that, the obtained product was gathered via filtration and drying. The as-prepared sample was denoted as OV-BOC.

2.2.2. Preparation of BiOCl without any oxygen vacancy

The synthesis procedure was similar with that of OV-BOC in addition to replacing EG with EtOH. The obtained sample was denoted as pure BOC.

2.2.3. Characterization

Crystalline structure analysis was carried out on X-ray diffraction (Cu Kα, Bruker-D8). The morphologies of the samples were characterized by scanning electron microscopy (SEM, Hitachi S-4800) and transmission electron microscopy (TEM, JEM-2100plus). The element composition and state were conducted on X-ray photoelectron spectroscopy (XPS, Axis supra). Diffused reflection spectra (DRS) were analyzed on UV–vis-near infrared light spectrophotometer (UV-3600 plus) with $BaSO_4$ as a reference. BET specific surface area tests were implemented on an ASAP 2050 apparatus. Zeta potential test was conducted on a Zeta potential analyzer (Zeta PALS). Fluorescence

spectrum analysis was performed on a fluorescence spectrometer (PL, FS5). Electrochemical impedance spectra (EIS) were obtained on electrochemical workstation (Chenhua 660D) with Na_2SO_4 as electrolyte. Detection of oxygen vacancy and reactive oxygen species were carried out on electron spin resonance spectrometer (ESR, EMXplus-10/12).

2.2.4. Photocatalytic activity tests

The photocatalytic properties were evaluated through the photodegradation of RhB, MO and phenol molecules under simulated sunlight. Photocatalytic reactions were took place in a 300 W Xenon lamp equipped with a UV cut-off filter ($\lambda > 400$ nm). Typically, 100 mg catalyst was added to 100 mL 10 mg L^{-1} RhB, MO or phenol aqueous solution. Prior to irradiation, the above suspension were agitated in darkness for 1 h to ensure that the equilibrium of adsorption-desorption had been built. After that, 3 mL of the suspension were taken out within given time interval. The concentration was measured by an ultraviolet-visible spectrophotometer and high performance liquid chromatography.

2.2.5. Radical species capturing experiments and quantitative analyses of $\cdot OH$, $\cdot O_2^-$ and $^1O_2$

For surveying the reactive species generated in photocatalytic process, isopropyl alcohol (IPA), 1,4-benzoquinone (BQ), ammonium oxalate (AO) and tryptophan (TRP) were served as quenchers of $\cdot OH$, $\cdot O_2^-$, h^+ and $^1O_2$, respectively. The procedure resembled the above photocatalytic ability tests in addition to adding 1 mM trapping agents. NBT (0.025 mM) with maximum absorption peak at 259 nm was to detect the yield of $\cdot O_2^-$ on ultraviolet-visible spectrophotometer. The concentration of $\cdot OH$ was monitored by measuring the fluorescence intensity of TA (0.5 mM) in KOH (2 mM) at excitation wavelength of 365 nm. The process was in the same method as above photodegradation experiments except that NBT and TA were employed to replace model organic pollutants.

2.2.6. ESR examinations

Direct reactive oxygen species (ROS) detections were performed on an electron spin resonance spectrometer. The detailed experimental sections are as follows: 500 μL catalyst sample (2 g / L) was added into DMPO solutions (500 μL, 0.1 M / L). Then xenon lamp was applied as a light source to monitor $\cdot O_2^-$ and $\cdot OH$. To measure the generated $^1O_2$, TEMP dissolved in HAc/NaAc buffer solution (pH = 3.5) was mixed with photocatalyst. Upon 3 min illumination, the mixture was then tested on ESR device.

3. Results and discussion

3.1. Characterization

3.1.1. Structures and morphologies

The phase structures of the obtained samples are confirmed by XRD patterns (Fig. 1). All sharp diffraction peaks of as-obtained samples are corresponding with tetragonal phase of BiOCl (standard card No. 06-0249) and no other superfluous peaks are watched, demonstrating the good crystallinity of samples. The half-peak width of OV-BOC sample is larger than the counterpart of BOC sample, implying its smaller particle diameter, which can be further confirmed by SEM images. More significantly, compared to pure BOC, the intensity of (00X) diffraction peaks (X = 1, 2) of OV-BOC sample is weakened which can be explained that EG inhibits the growth orientations along (00X) direction and the introduction of oxygen vacancy may induce the localization on (00X) plane.

The morphologies of as-obtained BOC and OV-BOC are observed by SEM and TEM. As depicted in Fig. 2a and b, the OV-BOC sample is comprised of hierarchical microspheres which are piled up by a large amount of nanosheets. The TEM image (Fig. 2e) also verifies this hierarchical structure and the average sizes are ranging from 1 μm to
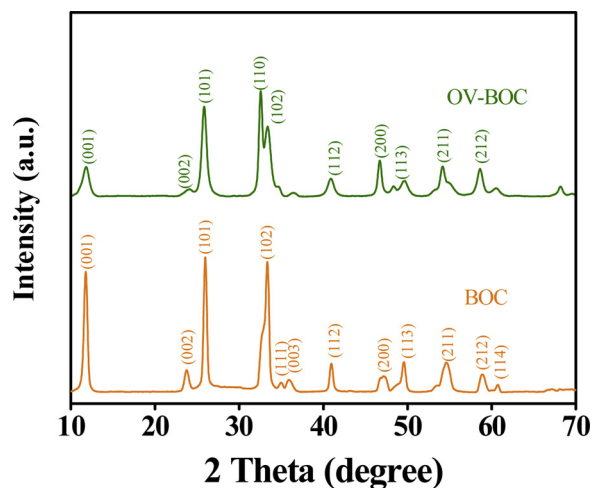
Fig. 1. XRD patterns of the synthesized OV-BOC and BOC samples.

1.5 μm. The HRTEM image (Fig. 2f) shows a clear crystal lattice whose spacing was about 0.275 nm, according with the (110) plane tetragonal BiOCl. The SEM image of BOC (Fig. 2c and 2d) reveal the irregular agglomerate nanoplate feature.

3.1.2. Oxygen vacancy

To identify the structure difference of OV-BOC and BOC, high resolution X-ray photoelectron spectroscopy (XPS) was conducted. As shown in Fig. 3a, pure BOC sample exhibits two intense characteristic peaks of Bi^{3+} $4f_{7/2}$ and Bi^{3+} $4f_{5/2}$ which locate at 158.9 eV and 164.2 eV, respectively. In contrast to pure BOC, characteristic peaks of Bi^{3+} in OV-BOC sample has a 0.3 eV offset to higher binding energies, which means the generation of oxygen vacancy [42]. The reason is that EG has mild reducibility [43] it would react with lattice oxygen in BiOCl to generate oxygen vacancy. For a more intuitive determination of the oxygen vacancy, electron spin resonance (ESR) measurement was applied. As depicted in Fig. 3b, an intense signal peak at g = 2.003 which is considered as the electrons trapped on oxygen vacancy [44,45] is merely discovered in OV-BOC sample, confirming the existence of oxygen vacancy in OV-BOC material.

3.1.3. Light absorbing abilities

Diffuse reflectance spectra of as-prepared samples are presented in Fig. 4. Obviously, pure BOC only presents intense absorption in ultraviolet domain. After introducing oxygen vacancy, the spectrum line of OV-BOC sample has a significant red-shift and defect characteristic of exponential attenuation around 400 nm, hence the photoabsorption can be broadened to visible-light region. The band gaps of as-obtained samples are determined using plot $(\alpha h\nu)^{1/2}$ versus $h\nu$ (where α, h, ν
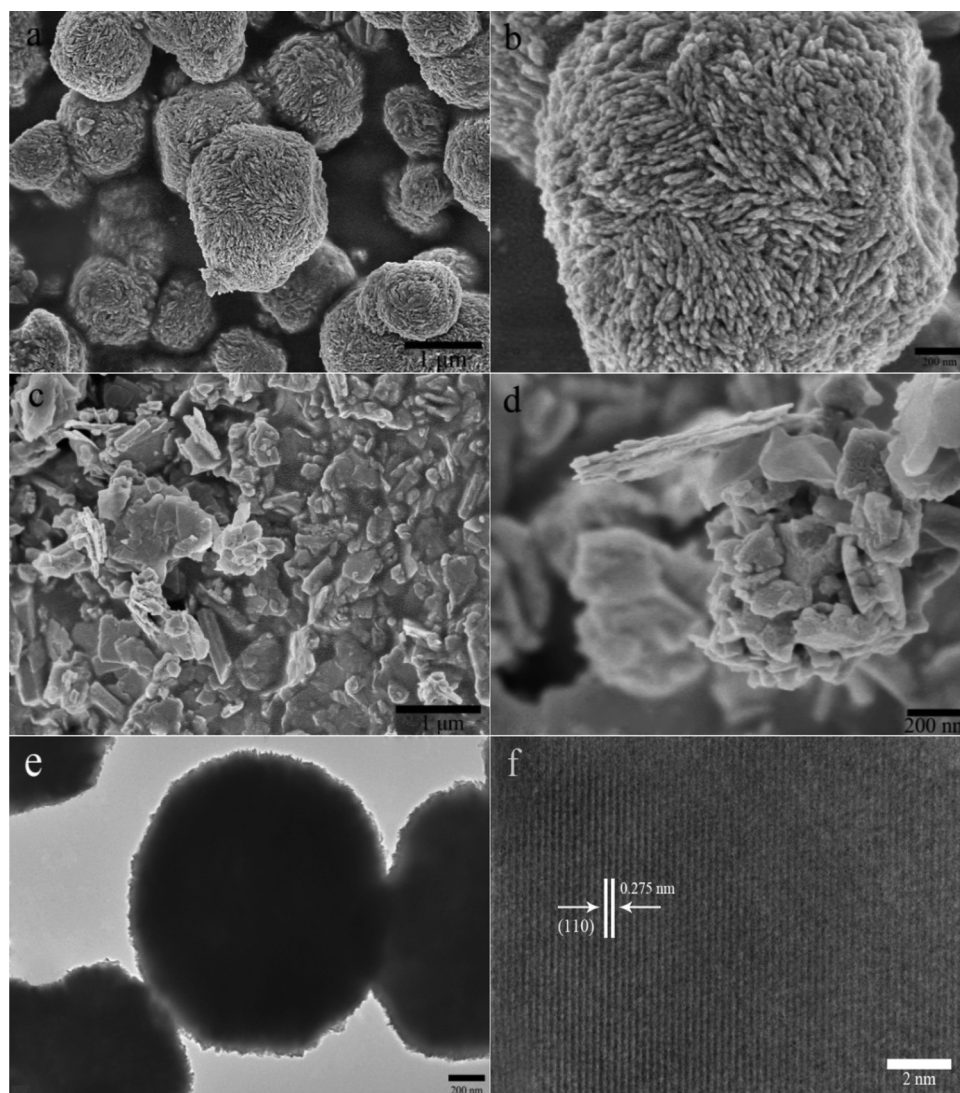

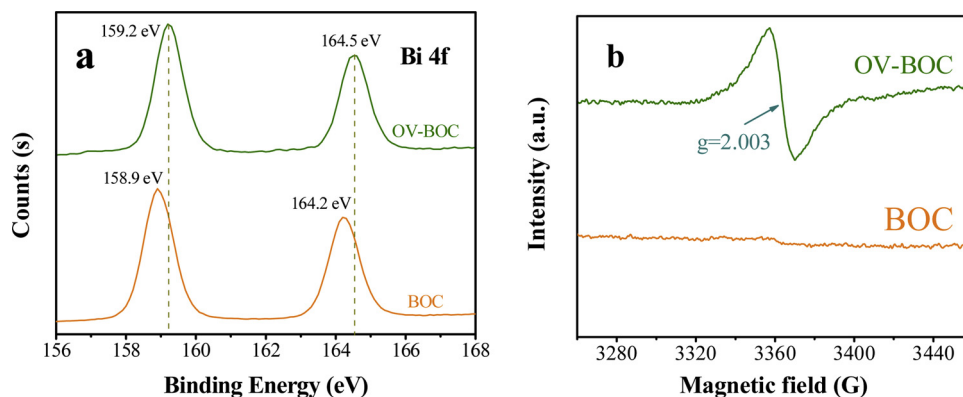**Fig. 2.** SEM images of OV-BOC (a, b) and BOC (c, d), and TEM (e) and HRTEM (f) images of OV-BOC.

Fig. 3. (a) High-resolution XPS spectra of Bi 4f and (b) ambient-temperature electron spin resonance (ESR) spectra.
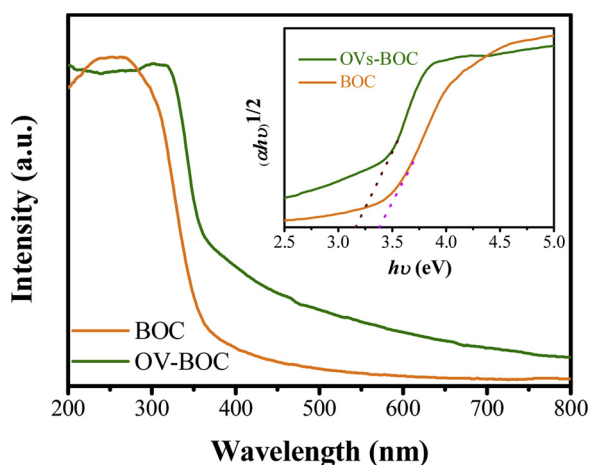

Fig. 4. DRS spectra and plots of $(ah\nu)^{1/2}$ versus $h\nu$ (insert) of the as-synthesized OV-BOC and BOC samples.

represent absorption coefficient, Planck constant, light frequency, respectively) [46] and the results are shown in the insert of Fig. 4. Visibly, the OV-BOC sample possesses a narrower band gap than BOC owing to oxygen vacancy [47].

3.1.4. BET surface areas and pore structure

It has been generally approved that specific surface area and pore structure greatly influence the photocatalytic process. N_2 adsorption-desorption isotherms (Fig. 5) revealed the type-IV adsorption feature, suggesting the existence of mesopore. The corresponding pore size
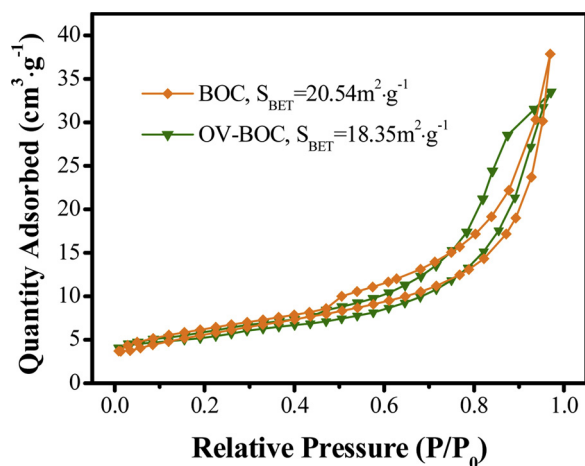

Fig. 5. N_2 adsorption-desorption isotherms curves of the as-prepared samples.

distribution is presented in Fig. S1. It can be found that mesopore and macropore are coexisted at the same time in both pure BOC and OV-BOC materials and the pore size are commonly distributed ranging from 20 nm to 150 nm. The comparison of BET surface area, pore volume and average pore size are summarized in Table S1. The BET surface areas of BOC and OV-BOC are 20.54 $m^2 g^{-1}$ and 18.35 $m^2 g^{-1}$, respectively, demonstrating no significant difference, which suggested that specific surface area was unconcerned with the photocatalytic activity in our case.

3.1.5. Photoluminescence and impedance analyses

PL and EIS are the common analytical tools to estimate the charge separation and migration [48,49]. As displayed in Fig. 6a, OV-BOC sample presents lower fluorescence intensity, verifying that the recombination rate is effectively inhibited because of the existence of oxygen vacancy. Equally, in Fig. 6b, OV-BOC owns smaller arc radius than BOC, indicating that the OV-BOC sample signifies minor interfacial charge transport resistance, thus leading to effective charge separation.

3.2. Photocatalytic degradation performance

The photocatalytic property investigations are probed by degrading different pollutant molecules under visible light illumination. As shown in Fig.7a, pure BOC has poor photodegradation ability towards RhB solutions due to its weak photoresponse. By comparison, the OV-BOC sample reveals remarkably enhanced photocatalytic ability and near 92% removal rate can be achieved. Especially, the RhB molecules can be completely degraded by OV-BOC sample with addition of 1 mM H_2O_2 upon 30 min exposure to illumination. The photodegradation of MO and phenol are also conducted and the results are depicted in Fig. 7b and 7c. Obviously, the variations of removal rate have a similar tendency towards the counterpart of RhB solutions. Slightly different, the photodegradation efficiency of MO and phenol is a little lower than that of RhB and this phenomenon can be explained that RhB molecules have an affinity for holes, [50] main active species in photodegradation process, which is further demonstrated in the latter part. To eliminate the effect of electrostatic action, zeta potential of OV-BOC sample is measured. In Fig. S2, the positive charge (+18.9 mV) indicates that zeta potential is not an influence factor of photocatalytic performance for OV-BOC has superior photodegradation ability towards cation pollutant (RhB). The above results indicate that both oxygen vacancy and H_2O_2 are advantageous to the removal of pollutants.

Furthermore, the kinetic curves using the plot of $\ln(C_0/C_t)$ versus illumination time (t) are displayed in Fig. 8a. We can intuitively discover that kinetic constants (k) of OV-BOC sample towards the degradation of RhB, MO and phenol have increased 2.6, 2.4 and 3.1 times, respectively when 1 mM H_2O_2 is added. The detailed numerical values of kinetic constants (k) of the as-obtained OV-BOC sample under different conditions are presented in Fig. 8b.
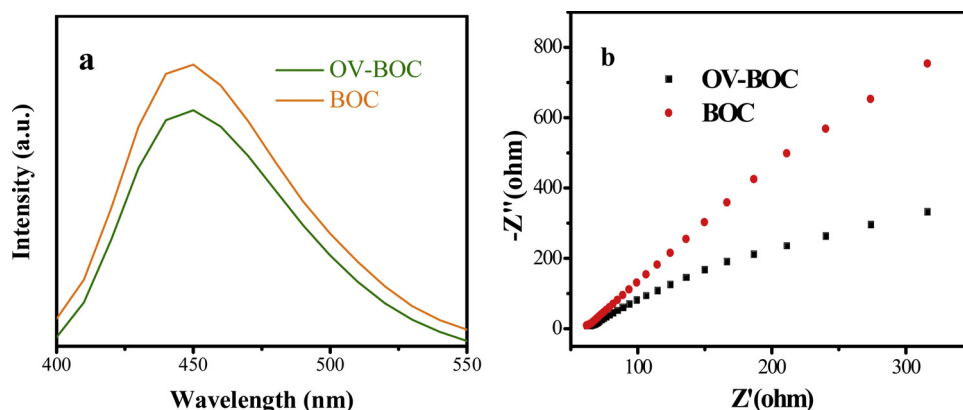
Fig. 6. (a) PL spectra and (b) EIS spectra of as-synthesized samples.

3.3. Reusability and stability

It is vital to evaluate the reusability and stability of the catalyst for its potential commercial application. Firstly, we conduct the cyclic experiment of the degradation of RhB. The cycling curves (Fig. S3) reveal that the photocatalytic performance after three cycles does not have significant decrease for both OV-BOC and OV-BOC/H_2O_2. Besides, XRD patterns comparisons (Fig. S4) before and after use are also made for determination of structural variation and expectedly almost no change can be observed. The above results demonstrate that OV-BOC/H_2O_2 may be a potential candidate for wastewater treatment application.

3.4. Investigations on the effect of H_2O_2 and oxygen vacancy on photodegradation

As we all know, H_2O_2 is an important active species which usually participate in photocatalytic degradation process [51], so it is essential to study the direct oxidation of pollutant substrates by H_2O_2. It can be clearly observed in Fig. 7a and b that sole H_2O_2 can barely oxidize pollutants molecules so we can rule out the direct oxidation of H_2O_2 which may be responsible in the process of photodegradation. Based on this, it can be inferred that H_2O_2 and oxygen vacancy play cooperative roles in efficient removal of different pollutants.

To better understand the synergy between H_2O_2 and oxygen vacancy, semiquantitative detection of $\cdot O_2^-$ and $\cdot OH$ in the presence or absence of H_2O_2 in the photocatalytic system is carried out. The yields of $\cdot O_2^-$ are determined by the concentrations of the consumption of NBT, the ratio between concentration of $\cdot O_2^-$ and consumption of NBT is 1:4 [52]. As exhibited in Fig. 9a, without addition of H_2O_2, the generation of $\cdot O_2^-$ of OV-BOC sample is mainly activated by localized electrons [53] through one-electron reduction ($O_2 + e^- \rightarrow \cdot O_2^-$). Interestingly, when adding 1 mM H_2O_2, the amount of $\cdot O_2^-$ is 2–3 times greater than the counterpart in the absence of H_2O_2. By contrast, the
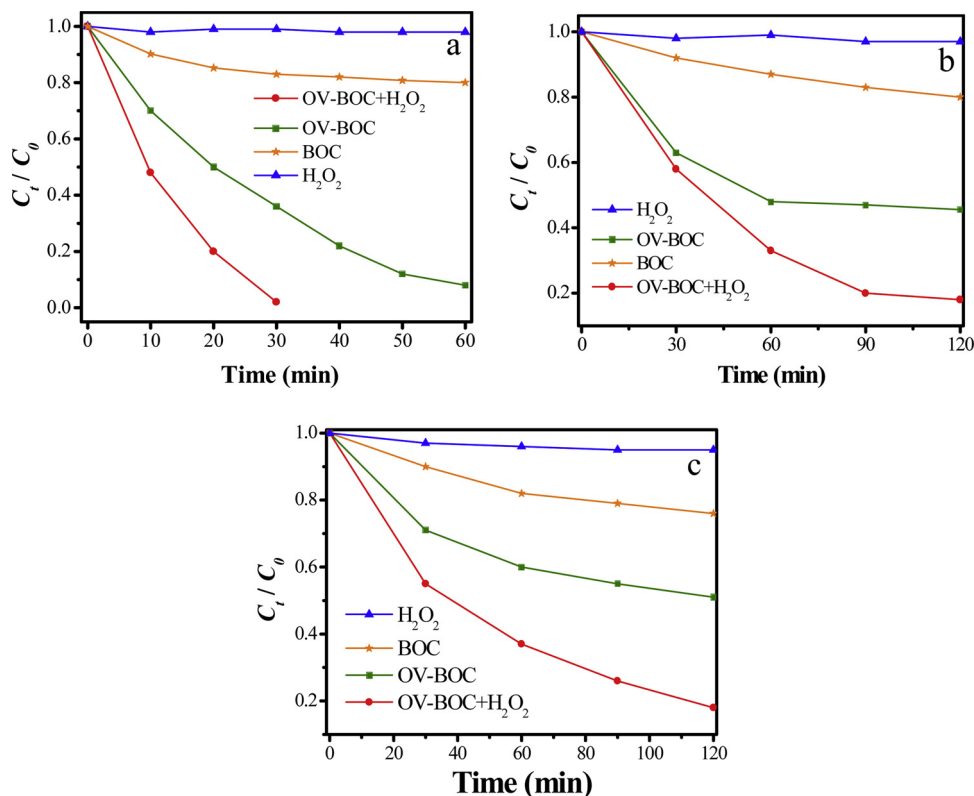

Fig. 7. Photocatalytic degradation experiments under different conditions of (a) RhB (b) MO and (c) phenol.
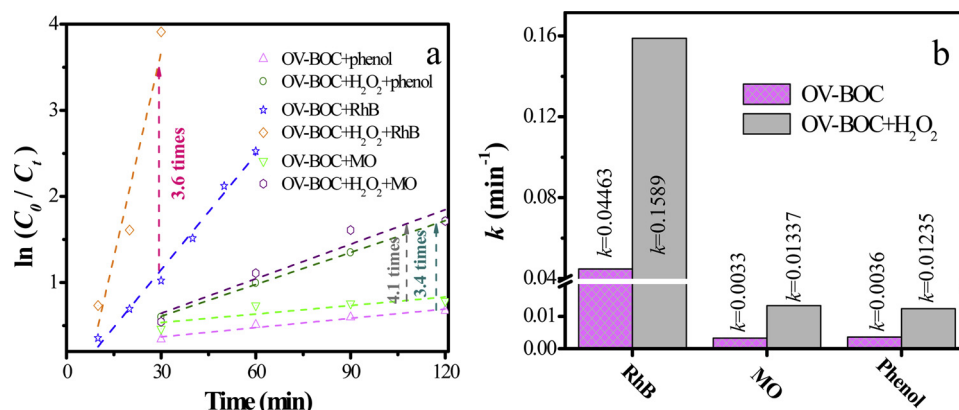
Fig. 8. (a) First-order kinetic curves and (b) comparison of apparent rate constant of the as-obtained OV-BOC sample under different conditions.

˙OH generation is analyzed by testing the fluorescence intensity of 2-hydroxy terephthalic acid (TAOH) at 425 nm [54,55]. As depicted in Fig. 9b, whether H_2O_2 is added or not, the fluorescence intensity is quite low, indicating that almost no ˙OH produce in the reaction system. However, it was confirmed by zhang et.al that oxygen vacancy could induce the dissociation with H_2O_2 to generate more ˙OH when the material was exposed to specific crystal facets [56]. This difference compared to Zhang's experiment is mainly due to the distinct of the surface structure and extremely low amount of H_2O_2 addition against this dissociation. According to the above results, it can be deduced that this reaction ($H_2O_2 \rightarrow \bullet OH$) by single electron reduction or other reaction pathway would not occur. The significantly increased formation of ˙O_2^- with the addition of H_2O_2 was attributed to the oxidation of H_2O_2 with a photoinduced valence-band hole (h^+). The generation process was illustrated in the equation: ($H_2O_2 + h^+ \rightarrow \bullet O_2^- + 2H^+$). Additionally, the consumption of holes may boost the separation of electron-hole pairs in the meanwhile which is advantageous to photocatalytic degradation [57].

To achieve comprehensive understanding of generation of ROS, the ESR tests are performed and the corresponding results are displayed in Fig. 10. Obviously, four strong peaks with intensity ratio of 1:1:1:1 are observed which are the characteristic peaks of ˙O_2^- signal (Fig. 10a). Furthermore, the addition of H_2O_2 contributes to an enhanced ESR signal, indicating that more production of ˙O_2^- is achieved. No discriminable signal of ˙OH is monitored even in the case of H_2O_2-containing system (Fig. 10b), further confirming the low content of ˙OH in photocatalysis. The aforementioned ESR results are in line with the former semiquantitative measurements of ˙O_2^- and ˙OH. In addition, the detection of $^1O_2$ with TEMP as spin-trapping agent is also explored. As illustrated in Fig. 10c, triplet signal peaks which are the features of $^1O_2$ are in sight. Besides, an insignificant increased intensity of $^1O_2$ signal is observed in H_2O_2 system, signifying a little more generation of

$^1O_2$. A deeper exploration of this phenomenon and the generation process of $^1O_2$ would be discussed in our following part.

Further investigations on the contributions of different active species are carried out by radical scavenging experiments. As displayed in Fig. 11, without adding any quenchers, the removal efficiency of RhB molecules can reach up to 98% and 92% in the presence/absence of H_2O_2, respectively. After the addition of 1 mM IPA served as trapping agent of ˙OH, the photocatalytic efficiency has been little decline, suggesting that ˙OH is not the main active species in the photodegradation system. This result parallels well with the former semiquantitative analyses of ˙OH. However, when adding 1 mM AO, BQ and TRP as quenchers of h^+, ˙O_2^- and $^1O_2$, an obvious suppression of photocatalytic efficiency has obtained, indicating that h^+, $^1O_2$ and ˙O_2^- are all responsible for RhB degradation. Especially for h^+, the photocatalytic efficiency

of OV-BOC/H_2O_2 and OV-BOC decreases by 99% and 97%, respectively. So we can conclude that h^+, $^1O_2$, ˙O_2^- species all have a large effect on photodegradation. One particularly considerable note: the role of $^1O_2$ in RhB photodegradation is similar to ˙O_2- which may eliminate the possibility that the generation of $^1O_2$ stemmed from the oxidation of ˙O_2- ($\bullet O_2^- + h^+ \rightarrow {}^1O_2$) [58]. If $^1O_2$ is generated through this process, the addition of the quencher of ˙O_2- would simultaneously shut down the formation of $^1O_2$ and thus leads to far stronger inhibition towards RhB degradation than $^1O_2$. Nevertheless, the fact was not like this. On the other hand, the measurement of $^1O_2$ was in TEMP buffer solution without the participation of RhB, eliminating the possibilities that dye molecules function as photosensitizer to realize the production of $^1O_2$ [59]. So it can be speculated that the generation of $^1O_2$ is owing to oxygen vacancy which lowers the energy barrier to support the process that ground state oxygen molecules are excited to single state reactive oxygen. Additionally, the observation, an obscure increase of $^1O_2$ generation with the addition of H_2O_2, may be explained that the

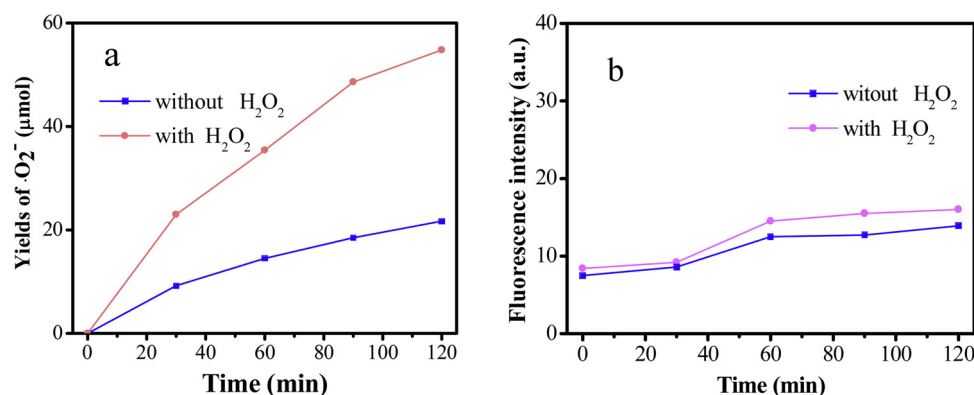**Fig. 9.** (a) Generation of ˙O_2^- free radicals and (b) fluorescence intensity of TAOH of OV-BOC photocatalyst in the presence or absence of H_2O_2.
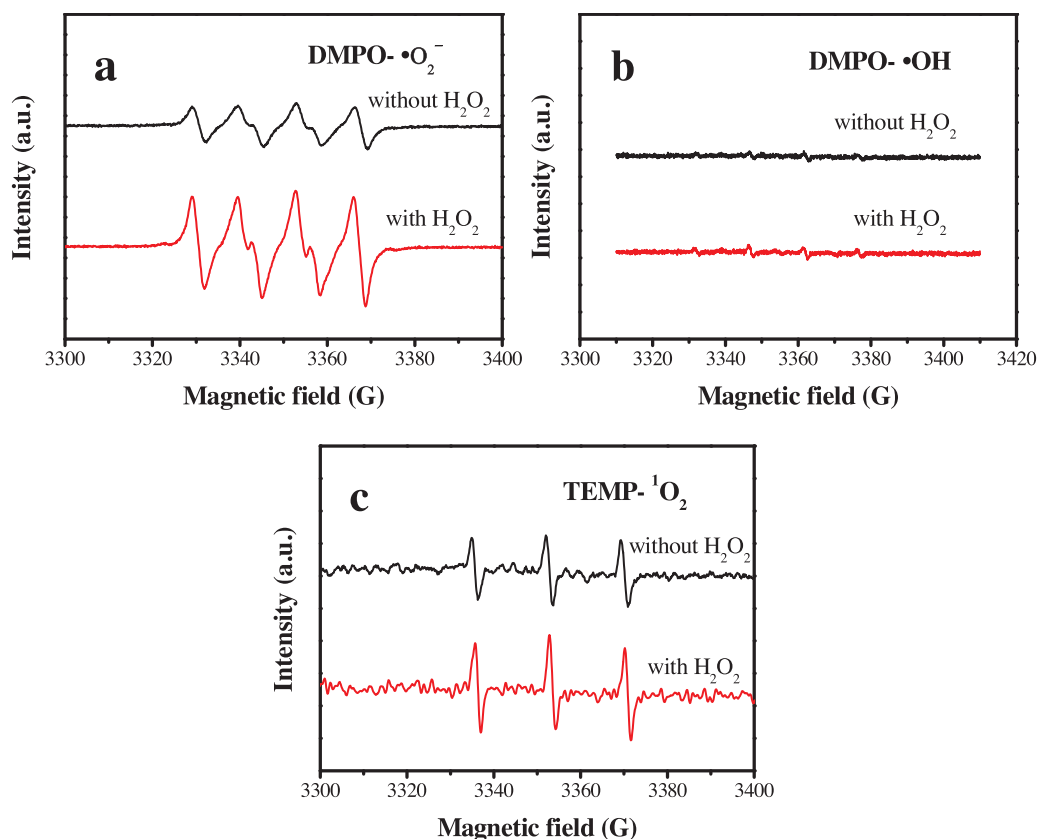
Fig. 10. ESR examinations of superoxide radicals (a), hydroxyl radicals (b) and singlet oxygen (c) upon 3 min illumination.
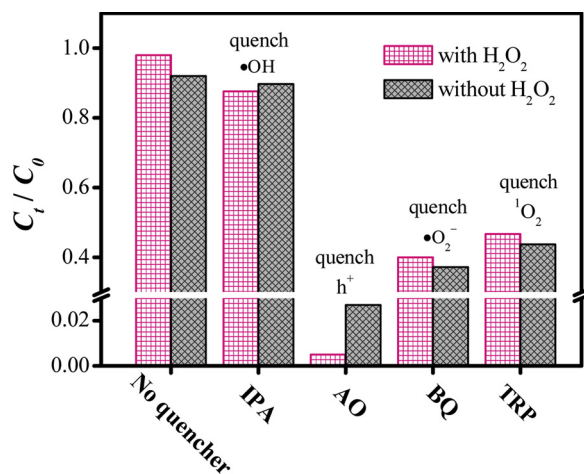

Fig. 11. Influence of each active species on photodegradation of RhB solution by OV-BOC sample under different conditions.

$^1O_2$ sorption on the catalyst surface is restrained because of the adsorption of H_2O_2 [57].

3.5. Band structure and photocatalytic mechanism for pollutants removal

It is well known that band structure has a great influence on the generation and migration of carriers. Valence band spectra of XPS (VB-XPS) of the as-obtained samples are achieved to investigate the valence band location. As shown in Fig. 12a, the pure BOC sample displays typical valance band DOS characteristic [42] and the position of VB is determined at 2.15 eV. On the basis of the equation: $E_{CB} = E_{VB} - E_g$ and the obtained band gap of BOC (Fig. 4), the potential of conduction band (CB) would occur at -1.23 eV. For the OV-BOC sample, the observation

of 0.17 eV down-shift of valance band can be easily found and the CB potential is determined likewise at -0.84 eV. The corresponding energy band structure is more directly revealed in Fig. 12b. Generally, a more positive VB potential signifies higher oxidation capacity of photo-generated holes. In our case, the down-shift of VB potential can lead to stronger oxidation capacity towards the removal of different pollutant molecules because h^+ make the major contribution in the photo-degradation process which is discussed above. Furthermore, it may accordingly induce an easier hole attack to generate more $^.O_2^-$ ($H_2O_2 + h^+ \rightarrow \cdot O_2^- + 2H^+$) which involved in the photodegradation process.

Herein, in view of the aforementioned analysis, the photocatalytic mechanism is put forward in Fig. 13. For BOC, the broad band gap makes it unable to absorb visible light so that it owns poor photo-catalytic activity. Nevertheless, when oxygen vacancy is introduced, a localized state emerged which broadens the photoabsorption to visible region [60]. Electrons in localized state would transfer to conduction band (CB) via interband excitation. Then, the electrons would be trapped by O_2 to generate $^.O_2^-$. In the meanwhile, oxygen vacancy may lower the energy barrier to support the formation process of $^1O_2$ which plays unnegligible role in photocatalysis. Compared with pure BOC, the as-obtained OV-BOC possesses a down-shift VB which is conductive to degrade pollutants by photogenerated holes with stronger oxidation ability. In addition, not only could H_2O_2 be activated by holes to produce $^.O_2^-$ but also decrease the $^1O_2$ sorption on the catalyst surface which accelerates photocatalytic degradation. These h^+, $^1O_2$ and $^.O_2^-$ species are responsible for pollutants removal. The reaction processes are illustrated as follows:

$$OV\text{-}BOC + h\nu \rightarrow h^+ + e^- \tag{1}$$

$$O_2 + e^- \rightarrow \cdot O_2^- \tag{2}$$

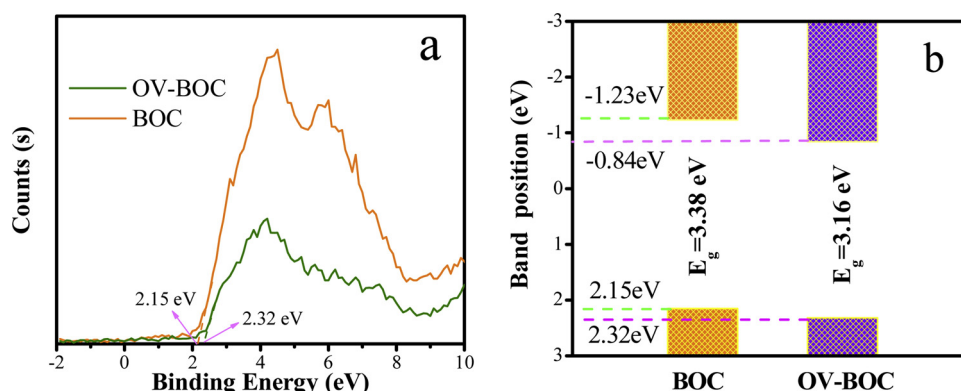$$3O_2 \xrightarrow{OV} {}^1O_2 \tag{3}$$

Fig. 12. (a) XPS valence band spectra and (b) the corresponding band position of as-obtained samples.
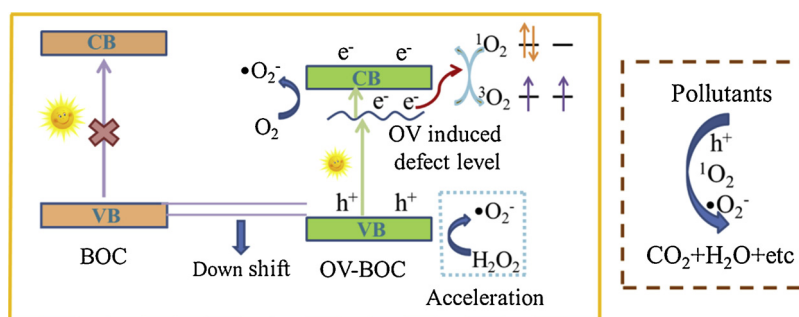
Fig. 13. Systematic illustration of photocatalytic mechanism.

$$Acceleration: H_2O_2 + h^+ \rightarrow \bullet O_2^- + 2H^+ \tag{4}$$

$$h^+ + 1O_2 + \bullet O_2^- + pollutents \rightarrow CO_2 + H_2O + etc \tag{5}$$
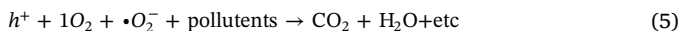
4. Conclusions

In conclusion, BiOCl with oxygen vacancy is prepared through a solvothermal modification method. Compared with pure BOC, the OV-BOC displays efficient removal efficiency towards different pollutant molecules. Especially, after adding a little H_2O_2, the degradation rate can be promoted by 2.6, 3.1 and 2.4 times towards RhB, MO and phenol, respectively. In view of numerous characterization results, this special solvothermal modification synthesis could not only introduce oxygen vacancy which is conductive to the generation of $^1O_2$ but made the VB down-shift and hence the photogenerated holes in VB owned stronger oxidation capacity. Expectedly, it is proved that these photo-generated holes contribute most to the photodegradation process. Moreover, the enhanced photodegradation performance in H_2O_2 system could be ascribed to the increased production of $\cdot O_2^-$ which may possibly originate from attack of hole with stronger oxidation capacity $(H_2O_2 + h^+ \rightarrow \bullet O_2^- + 2H^+)$. We expect that our discoveries may provide new ideas in energy band structure regulation and molecular oxygen activation for rational design of photocatalysts.

Conflict of interests

None.

Appendix A. Supplementary data

Supplementary material related to this article can be found, in the online version, at doi:https://doi.org/10.1016/j.apcatb.2019.117872.

References

[1] Z. Tong, D. Yang, J. Shi, Y. Nan, Y. Sun, Z. Jiang, ACS Appl. Mater. Interfaces 7 (2015) 25693–25701.
[2] F. Chen, Q. Yang, X. Li, G. Zeng, D. Wang, C. Niu, J. Zhao, H. An, T. Xie, Y. Deng, Appl. Catal. B 200 (2017) 330–342.
[3] H. Wang, L. Zhang, Z. Chen, J. Hu, S. Li, Z. Wang, J. Liu, X. Wang, Chem. Soc. Rev. 43 (2014) 5234–5244.
[4] Y. Feng, H. Li, L. Ling, S. Yan, D. Pan, H. Ge, H. Li, Z. Bian, Environ. Sci. Technol. 52 (2018) 7842–7848.
[5] B. Lin, H. Li, H. An, W. Hao, J. Wei, Y. Dai, C. Ma, G. Yang, Appl. Catal. B 220 (2018) 542–552.
[6] S. Zhu, W. Liao, M. Zhang, S. Liang, Chem. Eng. J. 361 (2019) 461–469.
[7] W. Zhang, G. Li, H. Liu, J. Chen, S. Ma, T. An, Environ. Sci. Nano 6 (2019) 948–958.
[8] G. Yi, X. Li, Y. Yuan, Y. Zhang, Environ. Sci. Nano 6 (2019) 68–74.
[9] Y. Feng, L. Ling, J. Nie, K. Han, X. Chen, Z. Bian, H. Li, Z.L. Wang, ACS Nano 11 (2017) 12411–12418.
[10] L. Ling, Y. Feng, H. Li, Y. Chen, J. Wen, J. Zhu, Z. Bian, Appl. Surf. Sci. 483 (2019) 772–778.
[11] T. Tachikawa, M. Fujitsuka, T. Majima, J. Phys. Chem. C 111 (2007) 5259–5275.
[12] G. Yin, X. Huang, T. Chen, W. Zhao, Q. Bi, J. Xu, Y. Han, F. Huang, ACS Catal. 8 (2018) 1009–1017.
[13] X. Chen, L. Liu, P.Y. Yu, S.S. Mao, Science 331 (2011) 746–750.
[14] Y. Zhang, M. Xu, H. Li, H. Ge, Z. Bian, Appl. Catal. B 226 (2018) 213–219.
[15] W. Li, X. Liu, H. Li, J. Mater. Chem. A 3 (2015) 15214–15224.
[16] S. Wang, D. Li, C. Sun, S. Yang, Y. Guan, H. He, Appl. Catal. B 144 (2014) 885–892.
[17] X. Liu, J. Zhang, Y. Dong, H. Li, Y. Xia, H. Wang, New J. Chem. 42 (2018) 12180–12187.
[18] L. Yang, L. Liang, L. Wang, J. Zhu, S. Gao, X. Xia, Appl. Surf. Sci. 473 (2019) 527–539.
[19] J.-G. Zhang, W.-J. Gong, Y.-S. Guan, H.-X. Li, D.J. Young, J.-P. Lang, Cryst. Growth Des. 18 (2018) 6172–6184.
[20] F. Wang, F.-L. Li, M.-M. Xu, H. Yu, J.-G. Zhang, H.-T. Xia, J.-P. Lang, J. Mater. Chem. A 3 (2015) 5908–5916.
[21] X.-Y. Wu, H.-X. Qi, J.-J. Ning, J.-F. Wang, Z.-G. Ren, J.-P. Lang, Appl. Catal. B 168 (2015) 98–104.
[22] M. Dai, H.-X. Li, J.-P. Lang, CrystEngComm 17 (2015) 4741–4753.
[23] M. Dai, X.-R. Su, X. Wang, B. Wu, Z.-G. Ren, X. Zhou, J.-P. Lang, Cryst. Growth Des. 14 (2014) 240–248.

[24] G.-J. Lee, Y.-C. Zheng, J.J. Wu, Catal. Today 307 (2018) 197–204.
[25] S. Garg, M. Yadav, A. Chandra, K. Hernadi, J. Nanosci. Nanotechnol. 19 (2019) 280–294.
[26] L. Yu, X. Zhang, G. Li, Y. Cao, Y. Shao, D. Li, Appl. Catal. B 187 (2016) 301–309.
[27] J. Lu, Y. Chen, L. Li, X. Cai, S. Zhong, L. Wu, J. Chen, S. Bai, Chem. Eng. J. 362 (2019) 1–11.
[28] B. Li, L. Shao, R. Wang, X. Dong, F. Zhao, P. Gao, Z. Li, J. Mater. Chem. A 6 (2018) 6344–6355.
[29] C.-Y. Wang, Y.-J. Zhang, W.-K. Wang, D.-N. Pei, G.-X. Huang, J.-J. Chen, X. Zhang, H.-Q. Yu, Appl. Catal. B 221 (2018) 320–328.
[30] Y. Mi, L. Wen, Z. Wang, D. Cao, R. Xu, Y. Fang, Y. Zhou, Y. Lei, Nano Energy 30 (2016) 109–117.
[31] M. Guan, C. Xiao, J. Zhang, S. Fan, R. An, Q. Cheng, J. Xie, M. Zhou, B. Ye, Y. Xie, J. Am. Chem. Soc. 135 (2013) 10411–10417.
[32] M. He, J. Ji, B. Liu, H. Huang, Appl. Surf. Sci. 473 (2019) 934–942.
[33] S. Tan, Y. Ji, Y. Zhao, A. Zhao, B. Wang, J. Yang, J.G. Hou, J. Am. Chem. Soc. 133 (2011) 2002–2009.
[34] M. Xu, Y. Chen, J. Qin, Y. Feng, W. Li, W. Chen, J. Zhu, H. Li, Z. Bian, Environ. Sci. Technol. 52 (2018) 13879–13886.
[35] V.J. Thannickal, B.L. Fanburg, Am J Physiol-lung C 279 (2000) L1005–L1028.
[36] J.F. Woolley, J. Stanicka, T.G. Cotter, Trends Biochem. Sci. 38 (2013) 556–565.
[37] Y. Su, X. Zhao, Y. Bi, C. Li, Y. Feng, X. Han, Environ. Sci. Nano 5 (2018) 2069–2076.
[38] Z. Xu, R. Zheng, Y. Chen, J. Zhu, Z. Bian, Chin. J. Catal. 40 (2019) 631–637.
[39] Y. Nosaka, A.Y. Nosaka, Chem. Rev. 117 (2017) 11302–11336.
[40] H. Huang, K. Xiao, S. Yu, F. Dong, T. Zhang, Y. Zhang, Chem. Commun. 52 (2015) 354–357.
[41] Q. Wang, W. Wang, L. Zhong, D. Liu, X. Cao, F. Cui, Appl. Catal. B 220 (2018) 290–302.
[42] D. Cui, L. Wang, K. Xu, L. Ren, L. Wang, Y. Yu, Y. Du, W. Hao, J. Mater. Chem. A 6 (2018) 2193–2199.
[43] Y. Wang, X. Li, F. Du, H. Yu, B. Jin, R. Bai, Chem. Commun. 48 (2012) 2800–2802.
[44] J. Wu, X. Li, W. Shi, P. Ling, Y. Sun, X. Jiao, S. Gao, L. Liang, J. Xu, W. Yan, C. Wang, Y. Xie, Angew. Chem. Int. Ed. 57 (2018) 8719–8723.
[45] X. An, Q. Tang, H. Lan, H. Liu, J. Qu, Appl. Catal. B 244 (2019) 407–413.
[46] Y. Ao, L. Xu, P. Wang, C. Wang, J. Hou, J. Qian, Dalton Trans. 44 (2015) 11321–11330.
[47] W.C. Huo, Xa. Dong, J.Y. Li, M. Liu, X.Y. Liu, Y.X. Zhang, F. Dong, Chem. Eng. J. 361 (2019) 129–138.
[48] L. Ye, X. Jin, Y. Leng, Y. Su, H. Xie, C. Liu, J. Power Sources 293 (2015) 409–415.
[49] H. Huang, K. Xiao, X. Du, Y. Zhang, ACS Sustainable Chem. Eng. 5 (2017) 5253–5264.
[50] D. Zhang, J. Li, Q. Wang, Q. Wu, J. Mater. Chem. A 1 (2013) 8622–8629.
[51] M. Fang, R. Zheng, Y. Wu, D. Yue, X. Qian, Y. Zhao, Z. Bian, Environ. Sci. Nano 6 (2019) 105–114.
[52] Y. Nosaka, A.Y. Nosaka, Chem. Rev. 117 (2017) 11302–11336.
[53] H. Li, F. Qin, Z. Yang, X. Cui, J. Wang, L. Zhang, J. Am. Chem. Soc. 139 (2017) 3513–3521.
[54] D. Xia, W. Wang, R. Yin, Z. Jiang, T. An, G. Li, H. Zhao, P.K. Wong, Appl. Catal. B 214 (2017) 23–33.
[55] D. Ma, J. Wu, M. Gao, Y. Xin, T. Ma, Y. Sun, Chem. Eng. J. 290 (2016) 136–146.
[56] H. Li, J. Shang, Z. Yang, W. Shen, Z. Ai, L. Zhang, Environ. Sci. Technol. 51 (2017) 5685–5694.
[57] T. Daimon, T. Hirakawa, M. Kitazawa, J. Suetake, Y. Nosaka, Appl. Catal. A 340 (2008) 169–175.
[58] D.R. Kearns, Chem. Rev. 71 (1971) 395–427.
[59] J. Agnieszka, K. Elzbieta, S. Grazyna, M. Wojciech, J. Am. Chem. Soc. 128 (2006) 15574–15575.
[60] H. Li, J. Li, Z. Ai, F. Jia, L. Zhang, Angew. Chem. Int. Ed. 57 (2018) 122–138.